Journal of Photochemistry and Photobiology A: Chemistry 228 (2012) 28–37

Contents lists available at SciVerse ScienceDirect

Journal of Photochemistry and Photobiology A: Chemistry

journal homepage: www.elsevier.com/locate/jphotochem

Spectroscopic and electrochemical studies on the interaction of an inclusion complex of β-cyclodextrin/fullerene with bovine serum albumin in aqueous solution

Mei-Fang Zhang[a], Li Fu[a], Jia Wang[a], Zi-Qiang Xu[a], Feng-Lei Jiang[a], Yi Liu[a,b,*]

[a] State Key Laboratory of Virology & Key Laboratory of Analytical Chemistry for Biology and Medicine (Ministry of Education), College of Chemistry and Molecular Sciences, Wuhan University, Wuhan 430072, PR China
[b] Department of Chemistry and Life Sciences, Xianning University, Xianning 437005, PR China

ARTICLE INFO

Article history:
Received 4 August 2011
Received in revised form
21 November 2011
Accepted 30 November 2011
Available online 8 December 2011

Keywords:
Functionalization
Fluorescence spectroscopy
Aqueous solution
$(\beta\text{-CD})_2/C_{60}$ complex
Bovine serum albumin

ABSTRACT

The potential effect of human exposure to carbonaceous nanomaterials (e.g., fullerenes or their derivatives) in the environment has become a concern. In the current study, we report the interaction of one water-soluble fullerene with bovine serum albumin using spectroscopic and electrochemical methods under aqueous solutions. The novel supramolecular inclusion complex of the water-soluble fullerene $(\beta\text{-CD})_2/C_{60}$ was synthesized and characterized. In the mechanism discussed, the spectroscopic methods such as fluorescence quenching and ultraviolet–visible absorption, proved that the fluorescence quenching of BSA by $(\beta\text{-CD})_2/C_{60}$ was the result of the formation of $(\beta\text{-CD})_2/C_{60}$–BSA complex and that the mechanism of quenching might be a static quenching procedure. The binding constants K_a, the number of binding sites n, and the corresponding thermodynamic parameters ΔG, ΔH, and ΔS at different temperatures were calculated through fluorescence spectroscopy, then as an auxiliary method, the electrochemical impedance spectroscopy (EIS) experiments confirmed this conclusion. The results indicated that the electrostatic interactions play a major role in $(\beta\text{-CD})_2/C_{60}$–BSA association. The circular dichroism spectra show the conformation change of the effect of $(\beta\text{-CD})_2/C_{60}$ on the conformation of BSA, which was confirmed by the results of the three-dimensional fluorescence spectra. Site marker competitive experiments indicate that the binding of $(\beta\text{-CD})_2/C_{60}$ to BSA primarily took place in site I. The distance r between donor (BSA) and acceptor ($(\beta\text{-CD})_2/C_{60}$) was obtained according to fluorescence resonance energy transfer (FRET). This work aims to demonstrate the mechanisms of the formation of the complex between water-soluble fullerene and protein under physiological conditions, as well as the remediation for the possible unwarranted biological effects of water-soluble fullerene.

1. Introduction

There is growing concern about the use of nanomaterials in the field of life science and biological applications, medicines and cosmetic ingredients, notably human exposure to carbonaceous nanomaterials (e.g., fullerenes) in the environment [1]. Nanomaterials are a very important basis for the future social development, and many new breakthroughs in the areas of science and technology urgently need the support of the nanomaterials and nanotechnology. C_{60}, one of the most promising nanomaterials, has been called a "radical sponge" [2] because of its extremely highly reactivity to radical species applicable in enzyme inhibition, antiviral activity, DNA cleavage, photodynamic therapy, electron transfer, etc. [3,4]. Scientists who engaged in fullerene research decades ago have made considerable progress. Generally, these works can be summarized as follows: (1) research on chemical properties of fullerenes, development of new chemical reactions and summary of the reaction rules; (2) modification of fullerene, in which by using fullerene as a platform and connecting it to groups with special functions, scientists have changed the electrical, optical, and magnetic properties of fullerene; and (3) increasing the water solubility of fullerenes to use their properties of anti-cancer and sterilization. In recent years, more and more research have focused on the performance of fullerene in biomedical applications, such as Friedman et al. [5], Nakamura and Isobe [6], Chiang et al. [7], among others.

However, their poor water solubility of fullerene has limited these biological applications. Recently, the water-soluble fullerenes have been obtained either by the non-covalent encapsulation of fullerene molecules in soluble polymeric or host molecules, or the reliance on covalent functionalization with hydrophilic groups by chemical modification [8]. As a common host molecule in the

* Corresponding author at: State Key Laboratory of Virology & Key Laboratory of Analytical Chemistry for Biology and Medicine (Ministry of Education), College of Chemistry and Molecular Sciences, Wuhan University, Wuhan 430072, PR China. Tel.: +86 27 68756667; fax: +86 27 68754067.
E-mail address: yiliuchem@whu.edu.cn (Y. Liu).

1010-6030/$ – see front matter © 2011 Elsevier B.V. All rights reserved.
doi:10.1016/j.jphotochem.2011.11.009

inclusion reaction, cyclodextrin (CD) is the amylase produced by bacillus cyclodextrin glycosyltransferase produced under the general term for a series of cyclic oligosaccharides. In the role of the cyclodextrin glycosyltransferase, CD constitutes a number of α-1,4-glycosidic bonds linked end to end generated by starch (mainly amylopectin) and usually contains 6–12 D-pyranose glucose units [9]. As the outer edge of the CD (rim) is hydrophilic and the cavity is hydrophobic, it has well-defined chemical structures with many sites for chemical modification or conjugation, which can provided a hydrophobic binding site as a main host for all appropriate guest. In this work, we successfully synthesized an excellent water-soluble fullerene derivative using CD.

As one of the most common and abundant carrier proteins, bovine serum albumin (BSA) has been widely applied in biology, physics, chemistry, medicinal chemistry, and computational chemistry studies, among others. As reported in [10,11], the distribution and metabolism of many biologically active compounds in the body are correlated with their affinity to serum albumin, and serum albumins are also found in tissues and body secretions throughout the body. Moreover, the extravascular protein comprises 60% of the total albumin [12]. Resent research reveals that various drugs can be significantly affected as a result of their binding to serum albumins in the circulatory system and that their interactions usually affect the secondary and tertiary structure of albumin. However, these drugs are often selected as small organic molecules, or low molecular weight dyes, and their ligands or derivatives, but nanomaterials are rarely selected, including carbonaceous materials. To this end, studying the interaction of nanomaterials with serum albumin is important. As the interactions between natural molecules and native proteins remain largely unexplored, as the great homologous protein of human serum albumins [10–12], BSA has been used widely as a model protein and has no exception in the current work.

The growing interest in fullerenes provides a compelling reason to investigate their interaction with proteins. Resent research have proved their interaction, such as the cholesterol modified fullerene/γ-cyclodextrin inclusion complex with BSA (HSA and DNA) [13], the polyhydroxylated fullerene derivative fullerol with BSA, etc. [14], the organophosphate-containing water-soluble derivative of fullerene with HSA [4], and the formation of a soluble stable complex between pristine fullerene and a native blood protein [15], among others. Although there is great interest in the biological effect of different drugs on protein especially in our group [11], the specific mechanism and conformational behavior of BSA changed by $(\beta\text{-CD})_2/C_{60}$ are poorly understood at present. Moreover, little work has been conducted to determine the poisonous and pharmacology adverse effect of fullerene. In this work, we first employ various experimental methods to detect comprehensively the influence of $(\beta\text{-CD})_2/C_{60}$ on the function and conformation change of BSA at the molecular level. We use several spectral methods to obtain information on the binding mechanisms of to BSA, such as quenching rate constant, binding modes, binding constants, binding number, binding sites, etc. We hope this study can provide valuable information to address the growing concern on the safety and toxicology of water-soluble fullerene derivatives, which have special molecular structures under physiological conditions and have become fundamental elements of biomedicine in future research.

2. Experimental details

2.1. Chemicals

BSA (defatted BSA, approx. 99%) and warfarin were obtained from Sigma–Aldrich (St. Louis, MO, USA); Ibuprofen was obtained from Hubei Biocause Pharmaceutical Co., Ltd. (Hubei, China; the purity no less than 99.7%); crystalline fullerene (C_{60}) powder of 99.9 wt.% purity was purchased from Yongxin Chemical Reagent Company. BSA was dissolved in Tris–HCl buffer solution with a purity of no less than 99.5% (0.05 mol L^{-1} of Tris, 0.10 mol L^{-1} of NaCl, and pH 7.4 ± 0.1). β-Cyclodextrin, N,N-dimethylformamide (DMF), sodium, naphthalene, iodine, and all other reagents and solvents used in synthesis and analysis were of analytical reagent grade and purchased from Sinopharm Group Chemical Reagent Company Ltd., Shanghai, P.R. China. Water used in all procedures was prepared using a Millipore water purification system. Sample masses were accurately weighted on a microbalance (Sartorius, ME215S) with a resolution of 0.1 mg.

2.2. Apparatus

The LS-55 spectrofluorophotometer from Perkin-Elmer equipped with a thermostat bath was used to measure all of the fluorescence spectras. The absorption spectra of the synthesized Inclusion Complex and BSA were recorded by a UNICO 4802 UV–vis double-beam spectrophotometer. The CD spectra were recorded on Cirsular Dichroism Photomultiplier from Applied Photophysics Limited, UK, using a cylindrical with 0.1 cm path length. The electrochemical properties studied were based on a CHI660C electrochemical workstation from Shanghai Chenhua Instrument Company. For characterizations, element analysis was measured on the 1112SERIES elemental analysis system produced by FLASH Company from Italy. The morphology and microstructure were observed by a scanning electron microscopy (SEM) with a Hitachi X-650. Infrared spectra were recorded on an Avatar 360 FT-IR spectrophotometer as KBr pellets. TGA analyses were performed in nitrogen with a temperature scanning rate of 10 K/min in a thermal analyzer of the NETZSCH STA 449C system. The crystal structures of the powers were characterized by X-ray diffraction analysis using Shimadzu XRD-6000 diffractometer with Cu Kα radiation (λ = 1.54056 Å). ^{13}C NMR spectra were recorded on mercury 600 MHz NMR spectrometer (Varian, Inc.) using the DMSO-d_6 as the solvent.

2.3. Preparation of water soluble fullerene $(\beta\text{-CD})_2/C_{60}$

The water-soluble derivative of C_{60}, two equivalents of β-cyclodextrin-bicapped C_{60}–fullerene inclusion complex ($(\beta\text{-CD})_2/C_{60}$) was synthesized by an improved method from Refs. [16,17] via the primary rim of the β-CD. Briefly, by using N,N-dimethylformamide (DMF) as the solvent, a certain amount of naphthalene (56 mg, 0.44 mmol) and elemental sodium (12 mg, 0.52 mmol) was added into the DMF solvent by a dry flask under the nitrogen atmosphere. After stirred for 6 h, sodium cannot be dissolved completely, and then a darker solution was achieved by soaking fullerene (30 mg, 0.04 mmol) into the flask with continuous stirring. β-Cyclodextrin (94.6 mg) was added into the solution to package fullerene after 12 h reaction. At last, iodine (17 mg, 0.07 mmol) was used to change the anion fullerene into neutral.

2.4. Fluorescence spectral measurements

All fluorescence spectra were measured on an LS55 fluorophotometer (Perkin-Elmer Co., USA) equipped with a 1.0 cm quartz cell and a thermostat bath. The widths of the excitation slit and the emission slit were set to 15 nm and 5.5 nm separately. An excitation wavelength of 295 nm was used throughout to minimize the contribution of the tyrosine residues to the emission. BSA solution was prepared on the basis of its molecular weight of 67,000 and kept in a refrigerator at 4 °C which was purchased from Sigma Aldrich and dissolved in PBS (pH 7.4) at the concentration of 2×10^{-6} mol L^{-1}.

The site-competitive replacement experiments were conducted by adding $(\beta\text{-CD})_2/C_{60}$ to the BSA-site marker system..

2.5. UV visible absorption spectra and circular dichroism spectra

The UV–visible absorption spectra were measured with a 1 cm quartz cell. The wavelength of the spectra was between 200 and 800 nm. The concentration of BSA and $(\beta\text{-CD})_2/C_{60}$ were 2.0×10^{-6} mol L^{-1}. The CD spectra were recorded on Jasco (J-810-150S) automatic recording spectropolarimeter, using a cylindrical cuvette with 0.1 cm of path-length under the condition of pH (7.4 ± 0.1) at 25 °C. The concentration of BSA was kept at 2.0×10^{-6} mol L^{-1} and the spectra were recorded from 200 to 240 nm, and the molar ratio of BSA/[$(\beta\text{-CD})_2/C_{60}$] was varied as 0:0, 1:1, 1:10, 1:25, 1:40, 1:50. From CD experiment, the content of the α-helix in the secondary structure of BSA was determined and the differential was compared.

2.6. Electrochemical impedance spectroscopy detection

2.6.1. Protein immobilization

The electrochemical analyzers were performed with a three-electrode configuration (CH Instruments Model 660C) from Shanghai Chenhua Apparatus Company. The working electrode was a bare or BSA-modified gold disk electrode (3 mm in diameter); a Pt wire and the Ag/AgCl electrode were utilized as counter and reference electrode, respectively. The BSA was tethered to the Au surface using the self-assembled method. Firstly, the working electrode was polished on chamois for 15 min and cleaned in acetone and ultrapure water respectively, then dried in nitrogen airflow. Then a tiny drop (approximately $4–5 \times 10^{-6}$ L) of BSA solution (2×10^{-6} mol L^{-1}) was dropped to the bare gold surface. At last, the electrode was washed by ultrapure water drop by drop several times and dried in nitrogen airflow after 18 h without hitting, and then the immobilization of BSA tiny layer was fabricated.

2.6.2. Electrochemical measurements

The electrolyte used in our experiments is a mixture of $K_3Fe(CN)_6/K_4Fe(CN)_6$ (5 mM) and KCl (10 mM) at pH 7.4. The EIS were measured within the frequency range from 0.1 to 10,000 Hz using the method of titration. Roughly, in order to ensure the success of the modification, firstly the BSA modified Au electrode was measured in the electrolyte to maintain balance for 15 min. Then different amount of the $(\beta\text{-CD})_2/C_{60}$ (1×10^{-3} mol L^{-1}) in aqueous solution was added continuously to the system and stirred for 1 min before testing to obtained the EIS spectra in Fig. 4(B).

3. Results and discussion

3.1. Characterizations of $(\beta\text{-CD})_2/C_{60}$

The schematic of the chemical structure of $(\beta\text{-CD})_2/C_{60}$ is presented in Scheme 1. The detailed characterizations of $(\beta\text{-CD})_2/C_{60}$ can be found in supporting information. According to the elemental analysis (Table S1), the atom ratio of carbon to hydrogen is about 1:1, which suggests that combination form of stoichiometry radio of CD:C_{60} is 2:1 in one inclusion complex. The absorption at 527 cm^{-1} can be clearly attributed to C_{60} and further suggests the modification is success from FT-IR spectra (Fig. S2) [18]. ^{13}C NMR spectrum (Fig. S6) illustrates that the interaction occurred in the primary face of CD, not in the secondary face [17], and that the binding ratio is in accordance with the elemental results combined with the TG-DSC (Fig. S3) analysis [18,19].

Scheme 1. The structure chart of $(\beta\text{-CD})_2/C_{60}$.

3.2. Interaction mechanism between $(\beta\text{-CD})_2/C_{60}$ and BSA

As we know, when an electron from a higher energy orbital returns to a lower orbital, the fluorescence is produced during the process. The interactions usually result in quenching and the mechanisms include excited-state reactions, molecular rearrangements, energy transfer, ground-state complex formation, collisional quenching, and so on [20]. Among these, the mechanisms are usually classified as either dynamic quenching or static quenching which can be distinguished by their differing dependence on temperature and viscosity, or excited-state lifetime.

In order to examine the interactions between $(\beta\text{-CD})_2/C_{60}$ and BSA were caused whether by $(\beta\text{-CD})_2/C_{60}$ or β-CD, fluorescence measurements were performed. In the experiment, the concentrations of BSA solution was stabilized at 2×10^{-6} mol L^{-1}, and the concentrations of $(\beta\text{-CD})_2/C_{60}$ and β-CD were varied from 0 to 4.5×10^{-6} mol L^{-1} at increments of 0.5×10^{-6} mol L^{-1}. The fluorescence spectra of BSA obtained in the presence of increasing amounts of $(\beta\text{-CD})_2/C_{60}$ and β-CD are shown in Fig. 1(A) and (B). The addition of $(\beta\text{-CD})_2/C_{60}$ led to a gradual decrease in the fluorescence intensity of BSA, while the β-CD only caused a slight change, which imply that addition of β-CD cannot change the polarity of the hydrophobic microenvironment around tryptophan in BSA. To study the quenching process by $(\beta\text{-CD})_2/C_{60}$ carefully, fluorescence tests have been performed at different temperatures. Higher temperatures result in faster diffusion and hence larger amounts of dynamic quenching. Higher temperatures will typically result in the dissociation of weakly bound complexes and, hence, smaller amounts of static quenching [21].

The data are analyzed using the well-known Stern–Volmer equation [22] (Eq. (1)):

$$\frac{F_0}{F} = 1 + K_{SV}[Q] = 1 + k_q \tau_0 [Q] \quad (1)$$

where F_0 and F denotes the steady-state fluorescence intensities in the absence or presence of quencher ($(\beta\text{-CD})_2/C_{60}$), respectively, K_{SV} is the Stern–Volmer quenching constant and [Q] is the concentration of the quencher. Hence, Eq. (1) was applied to determine K_{SV} by linear regression of a plot of F_0/F against [Q]. The calculation of K_{SV} from Stern–Volmer plots (Table 1) demonstrated the effect on fluorescence quenching by $(\beta\text{-CD})_2/C_{60}$ at each temperature (295, 300, and 305 K) were studied; the result indicates that the Stern–Volmer quenching constant K_{SV} decreases with increasing the temperatures (Fig. 2), which means the interactions between $(\beta\text{-CD})_2/C_{60}$ and BSA reaction are initiated by compound formation rather than by dynamic collision.

The ground-state complex formation frequently results in the perturbation of the absorption spectrum of the fluorophore, while the collisional quenching only affects the excited fluorophores, thus

Table 1
Stern–Volmer quenching constants for the interaction of $(\beta\text{-CD})_2/C_{60}$ with BSA at various temperatures.

pH	T (K)	$10^{-5}K_{SV}$ (L mol^{-1})	R^a	$S.D.^b$
7.4	295	3.662	0.9973	0.043
	300	3.552	0.9963	0.049
	305	3.220	0.9971	0.039

[a] R is the correlation coefficient.
[b] $S.D.$ is the standard deviation.

causing no change in the absorption spectra [23]. Thus, the UV–vis absorption spectra of BSA, $(\beta\text{-CD})_2/C_{60}$ and $(\beta\text{-CD})_2/C_{60}$–BSA systems are measured to confirm the quenching mechanism (Fig. 3). In Fig. 3, curve C (the difference in absorption spectra between [$(\beta$-CD)$_2/C_{60}$]–BSA and $(\beta\text{-CD})_2/C_{60}$, namely, the [$(\beta\text{-CD})_2/C_{60}$]–BSA] minus $(\beta\text{-CD})_2/C_{60}$), is obviously different from curve B (the absorption spectra of BSA only), especially around 230 nm. This result confirms that the quenching is mainly a static quenching process and is primarily caused by complex formation between $(\beta\text{-CD})_2/C_{60}$ and BSA.

EIS experiments are performed using a freshly prepared solution of electrolyte [in $K_3Fe(CN)_6/K_4Fe(CN)_6$ (5 mM) and KCl (10 mM)]. Comparing the EIS of bare Au electrode (Fig. 4(A)A) and BSA modified Au electrode (Fig. 4(B)B, the electron transportation become hard due to the successful immobilization of BSA. Fig. 4(B) shows the results of the corresponding experiment with increasing concentration of $(\beta\text{-CD})_2/C_{60}$ in the Au electrode that modified by BSA (Fig. 4(B)C–K) under the equilibrium interaction condition. The EIS in Fig. 4(B) reveals a regular increase of R_{ct} value by adding $(\beta$-CD$)_2/C_{60}$ to the electrochemical system continuously, as illustrated in the trend of the semicircle in the same figure. The total resistance also increases. This trend together with the changes in UV–vis experiments indicate that the mechanism between the interaction of $(\beta\text{-CD})_2/C_{60}$ and BSA is mainly a new complex formation process and not a collision, for the electronic conductive of the electrode modified by BSA has been obstructed seriously.

For accurate detect the influence of the blocking by adding $(\beta$-CD$)_2/C_{60}$, the affinity constant (K_A) was determined by recording equilibrium binding to the probe surface at different target concentrations C_0 through the Langmuir adsorption isotherm [24] (Eq. (2)):

$$R_{ct} = (R_{ct})\max \cdot c_0 \cdot \frac{K_A}{1 + c_0 \cdot K_A} \quad (2)$$

a plot of c_0/R_{ct} as a function of c_0 yields a straight line from which the affinity constant $K_A = 2.98 \times 10^5$ L mol^{-1} was deduced as shown in Fig. 5, and the linear correlation reached to 99.76%. K_A is a little higher than K_a (Table 2). This difference should be attributed to the nonspecific adsorption in the EIS test, whereas the binding mainly occurs around the tryptophan residue of BSA in the fluorescence experiment. In all, this value is generally in agreement with result from the fluorescence technique within the experimental error.

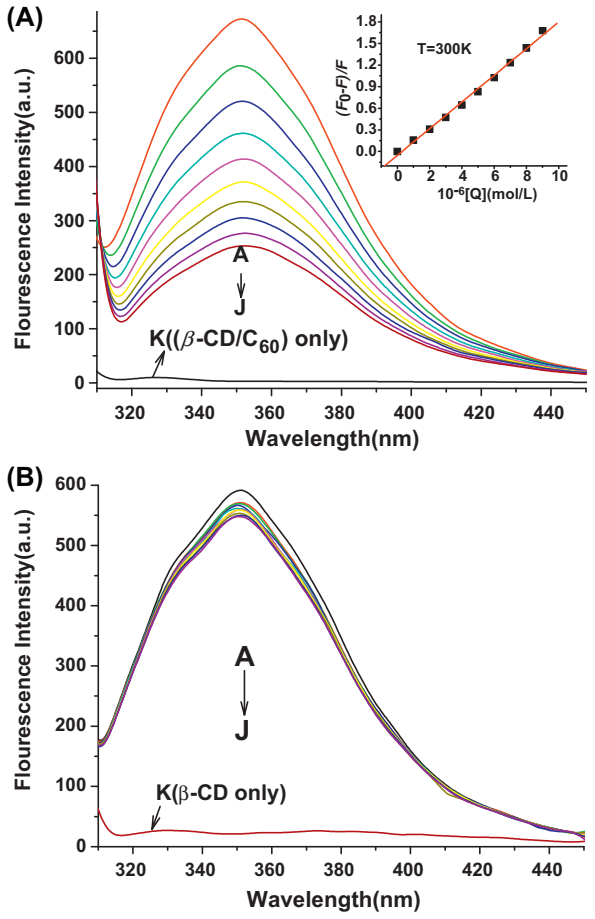

Fig. 1. Emission spectra of BSA in the presence of various concentrations of $(\beta\text{-CD})_2/C_{60}$ (A) and β-CD (B) at 300 K. c(BSA) = 2×10^{-6} mol L^{-1}, c((β-CD$)_2/C_{60}$)/(10^{-6} mol L^{-1}), c(β-CD)/(10^{-6} mol L^{-1}), A–J: from 0.0 to 4.5 at increments of 0.50. The curve K shows the emission spectrum of $(\beta\text{-CD})_2/C_{60}$ and β-CD only under the same condition. The insert corresponds to the Stern–Volmer plot.

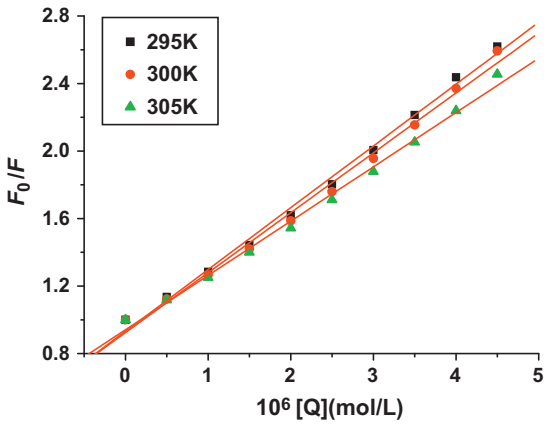

Fig. 2. Stern–Volmer plots for the quenching of BSA by $(\beta\text{-CD})_2/C_{60}$ at different temperatures.

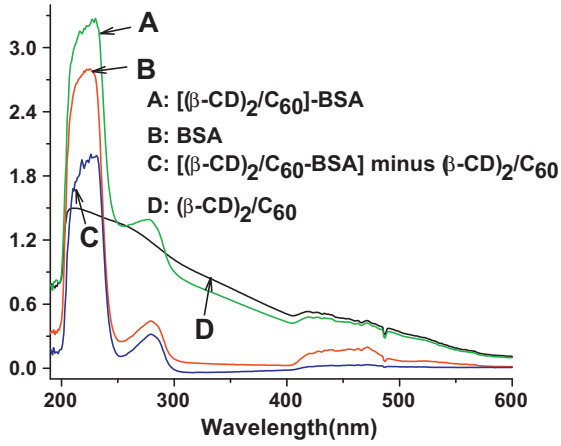

Fig. 3. Effect of [$(\beta\text{-CD})_2$]/C_{60} on ultraviolet absorption spectra of BSA. c(BSA) = c[(β-CD$)_2/C_{60}$] = 2 μM (298 K).

Table 2
Binding constants and relative thermodynamic parameters of BSA–$(\beta$-CD$)_2$/C_{60} interaction at pH 7.4.

pH	T (K)	$10^{-5}K_a$ (L mol^{-1})	R^a	$S.D.^b$	ΔH (kJ mol^{-1})	ΔS (J mol^{-1} K^{-1})	ΔG (kJ mol^{-1})	R^c	$S.D.^d$
7.4	295	1.920	0.9999	0.019	−20.494	31.768	−29.839	0.9950	0.013
	300	1.610	0.9998	0.039			−29.791		
	305	1.264	0.9992	0.109			−29.787		

[a] R is the correlation coefficient for modified Stern–Volmer plots.
[b] $S.D.$ is the standard deviation for modified Stern–Volmer plots.
[c] R is the correlation coefficient for van't Hoff plots.
[d] $S.D.$ is the standard deviation plots for van't Hoff.

The fluorescence quenching measurements, and the changes in UV–vis spectras together with the EIS experiments, confirm that the functionalization between $(\beta$-CD$)_2$/C_{60} and BSA follows the static quenching process, which forms a new complex rather than a dynamic collision. Therefore, the quenching data were analyzed according to the modified Stern–Volmer equation [25] (Eq. (3)):

$$\frac{F_0}{\Delta F} = \frac{F_0}{F_0 - F} = \frac{1}{f_a K_a}\frac{1}{[Q]} + \frac{1}{f_a} \tag{3}$$

where ΔF is the difference in fluorescence intensity between the absence and presence of quencher at concentration $[Q]$, f_a is the mole fraction of solvent-accessible fluorophore, and K_a is the effective quenching constant for the accessible fluorophores. The dependence of $F_0/\Delta F$ on the reciprocal value of the quencher concentration $[Q]^{-1}$ is linear, with slope equal to the value of $(f_a \cdot K_a)^{-1}$. The value f_a^{-1} is fixed on the ordinate. The constant K_a is the quotient of the ordinate f_a^{-1} and the slope $(f_a \cdot K_a)^{-1}$. Compared with the gamma-CD/fullerene with BSA [13], the association constant studied here is higher than that, which can be ascribed to the different synthesis reaction as well as the different methods in data processing. Fig. 6 displays the modified Stern–Volmer plots. The corresponding value of K_a at different temperatures is presented in Table 2. The decreasing trend of K_a with the increasing temperatures is in accordance with K_{SV}'s dependence on temperature as mentioned above, which coincides with the static quenching mechanism.

3.3. Type of interaction force

In general, the interaction forces between drugs and protein may include hydrogen bond, hydrophobic force, van der Waals forces, electrostatic interactions, and steric contacts within the antibody-binding site and so on [26]. To elucidate the interaction between and BSA, the temperature-dependent thermodynamic parameters were calculated from the van't Hoff plots. Supposed that the enthalpy change (ΔH) does not vary significantly in the

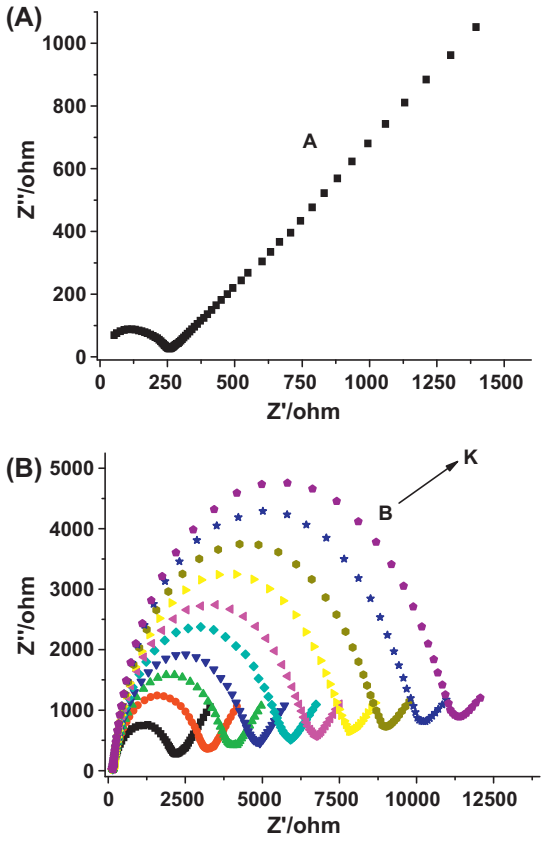

Fig. 4. Electrochemical impedance spectroscopy (EIS) of $(\beta$-CD$)_2$/C_{60} and BSA system. (A) EIS of bare Au electrode (A), (B) EIS of BSA modified Au electrode (B) and various volume of $(\beta$-CD$)_2$/C_{60} dropping into the BSA (C–K). The volume of B–K (μL): 0, 40, 50, 60, 70, 80, 90, 100, 110 and 120. c[$(\beta$-CD$)_2$/C_{60}] = 1×10^{-3} mol L^{-1} in aqueous solution.

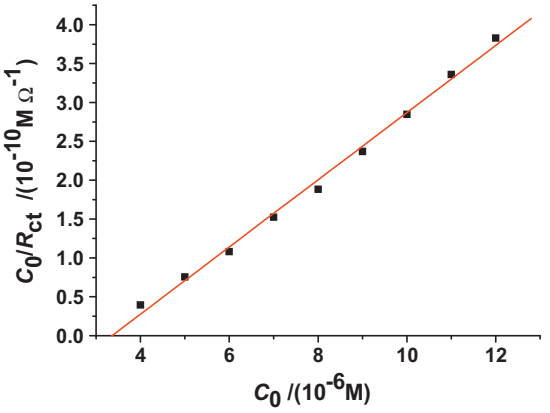

Fig. 5. Plot of Langmuir absorption isotherm model for $(\beta$-CD$)_2$/C_{60} and BSA system.

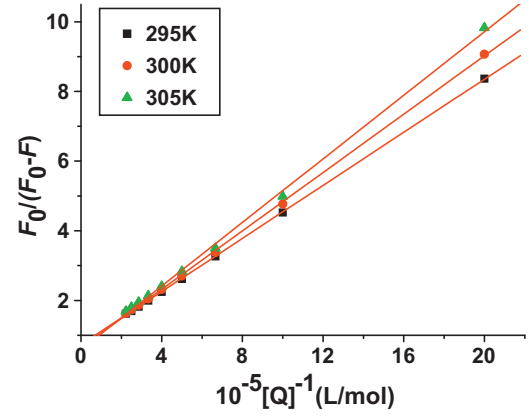

Fig. 6. The modified Stern–Volmer plots for the quenching of BSA by $(\beta$-CD$)_2$/C_{60} at different temperatures.

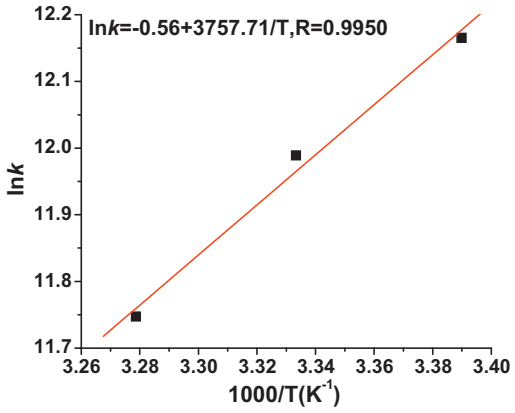

Fig. 7. Plots of van't Hoff equation of (β-CD)$_2$/C$_{60}$ and BSA at different temperatures, pH 7.4, c(BSA) = 2 μM.

temperature rang studied and that it can be considered constant, then both the enthalpy change (ΔH) and entropy change (ΔS) can be evaluated from the van't Hoff equation (Eq. (4)):

$$\ln K = -\frac{\Delta H}{RT} + \frac{\Delta S}{R} \quad (4)$$

where K is the analogous to the effective quenching constants at the corresponding temperatures and R is the gas constant. The temperatures used in our experiment were 295, 300 and 305 K. From Fig. 7 we can see that the linear relationship between ln K and 1/T is good. The enthalpy change (ΔH) is obtained from the slope of the van't Hoff relationship, while the energy change (ΔG) is then calculated from the following relationship (Eq. (5)):

$$\Delta G = \Delta H - T\Delta S = -RT \ \ln K \quad (5)$$

The corresponding results were presented in Table 2, while the values of ΔH and ΔS obtained of the binding site from the slops and ordinates at the origin of fitted lines. The values of ΔH and ΔS are found to be −20.494 kJ mol^{-1} and 31.768 J mol^{-1} K^{-1}, which indicated that the electrostatic interactions played an major role in the process of forming the BSA–(β-CD)$_2$/C$_{60}$ complex. The negative sign for ΔG means that the binding process is spontaneously driven by enthalpy and entropy together. Moreover, previous studies [27] showed that during the conjugation of nanoparticles with protein, other types of forces such as hydrophobic interactions and coordination binding might work besides electrostatic interactions.

3.4. Binding number and binding site on BSA

3.4.1. Binding number

Since there is a new formation of complex during the process of the interaction between (β-CD)$_2$/C$_{60}$ and BSA, the binding number between them has also been studied through the following double-logarithmic equation [28] (Eq. (6)):

$$\log\left(\frac{F_0 - F}{F}\right) = \log K_b + n \log[Q] \quad (6)$$

where F_0 and F stands to the fluorescence intensity in the absence and presence of quencher at various concentration of [Q] respectively, K_b refers to the binding constant, n is the binding number. According to the equation, the binding number can be obtained from the slop of the plot of log[($F_0 - F$)/F] vs. log[Q]. Fig. 8 demonstrates that the linear relationship is good and the value of n is close to 1, which suggests the water-soluble fullerene and BSA have a strong binding during their interaction process.

Table 3
Parameters of the site competitive replacement experiments.

Site marker	K_a (10^5 L mol^{-1})	R[a]	$S.D.$[b]
Blank	1.610	0.9998	0.039
Warfarin	0.696	0.9994	0.110
Ibuprofen	1.337	0.9997	0.079

[a] R is the correlation coefficient for modified Stern–Volmer plots.
[b] $S.D.$ is the standard deviation for modified Stern–Volmer plots.

3.4.2. Binding site competition experiment

In the site marker competitive experiment, warfarin and ibuprofen were used as site marker fluorescence probes for monitoring site I and site II of BSA respectively. Since (β-CD)$_2$/C$_{60}$ and BSA have one binding number, to clarify the specific binding location, we used drugs (warfarin and ibuprofen) to bind specifically bind to a known site or region on BSA. Information about the specific binding site can be gained by monitoring the changes in the fluorescence of (β-CD)$_2$/C$_{60}$-bound BSA brought about by site I and site II markers [29].

The mixture of ibuprofen–BSA or warfarin–BSA was titrated with (β-CD)$_2$/C$_{60}$. The fluorescences spectra were recorded upon excitation at 285 nm, and the quenching data were analyzed according to the modified Stern–Volmer equation (Eq. (3)). The corresponding results are shown in Table 3, indicating that ibuprofen has little influence on the binding of (β-CD)$_2$/C$_{60}$ to BSA, whereas the binding constant is surprisingly variable in the presence of warfarin. Fig. 9 shows the comparison of the fluorescence spectra of the BSA–(β-CD)$_2$/C$_{60}$ system with the ibuprofen and warfarin. The fluorescence property of the BSA–(β-CD)$_2$/C$_{60}$ system was almost the same as in the absence of ibuprofen. In contrast, in Fig. 9(B), the maximum emission wavelength of BSA has an obvious red shift (from 351 to 358 nm), and the fluorescence intensity is significantly higher than that without warfarin. The fluorescence intensity of the BSA decreased gradually with the addition of (β-CD)$_2$/C$_{60}$, and the wavelength emission maximum λ_{max} also had a red shift (from 358 to 363 nm). These results indicated that the binding of (β-CD)$_2$/C$_{60}$ to BSA was obviously affected by the addition of warfarin. The polar of the region surrounding the trypyophan site (Try-214) [30] was also increased. As discussed above, the results and plots demonstrated that the decrease in probe fluorescence may result from the competitive displacement of the probe and (β-CD)$_2$/C$_{60}$ bind with high affinity to site I (subdomain IIA) of BSA.

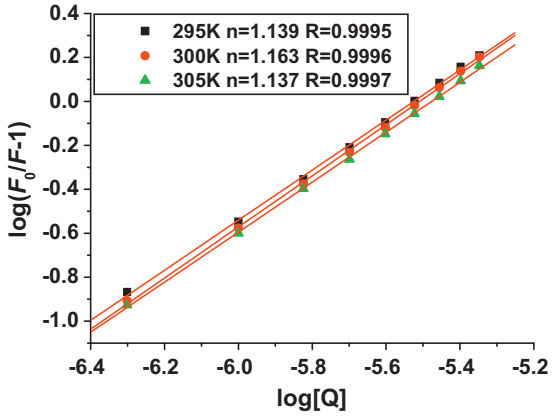

Fig. 8. Double-log plots of (β-CD)$_2$/C$_{60}$ quenching effect on BSA fluorescence at different temperatures.

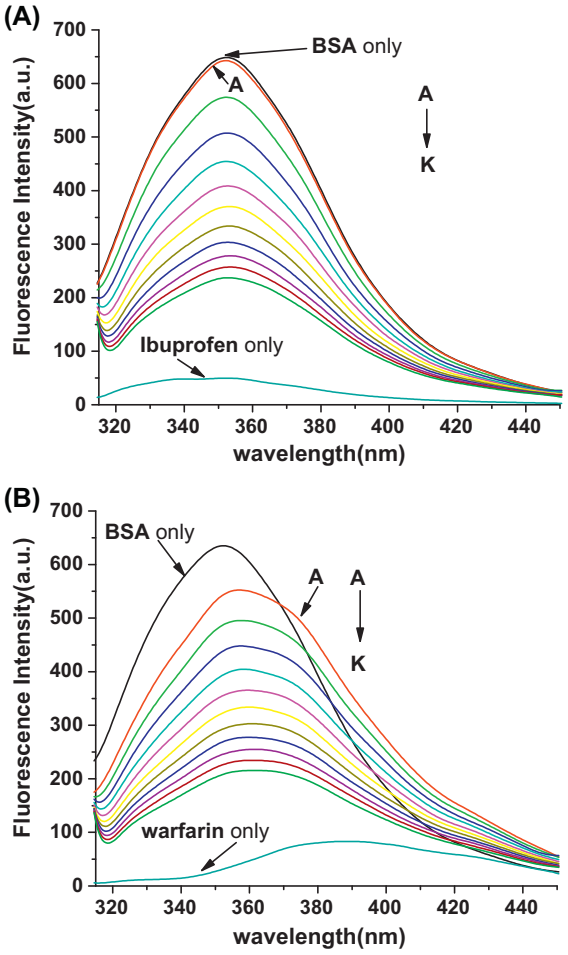

Fig. 9. Effect of site marker to the $(\beta\text{-CD})_2/C_{60}$–BSA system ($T$ = 300 K, λ_{ex} = 295 nm), c(ibuprofen) = c(warfarin) = c(BSA) = 2.0×10^{-6} mol L^{-1}; $c((\beta\text{-CD})_2/C_{60})/(2.0 \times 10^{-6})$, A–K: 0; 0.25; 0.50; 0.75; 1.00; 1.25; 1.50; 1.75; 2.00; 2.25; 2.50. The curve in the bottom shows the emission spectrum of ibuprofen (A) and warfarin (B) only in this condition.

3.5. Energy transfer between $(\beta\text{-CD})_2/C_{60}$ and bovine serum albumin

Considering the overlap between the emission spectra of BSA and the absorption spectrum of $(\beta\text{-CD})_2/C_{60}$ (Fig. 10), an excitation energy transfer mechanism might be assumed and such mechanism is very common. The theory of FRET (Fluorescence Resonant

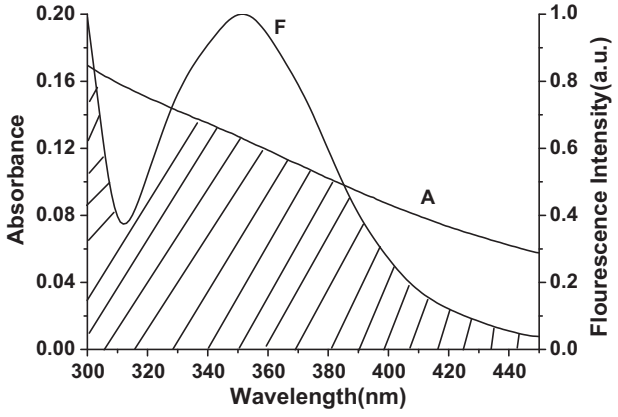

Fig. 10. The overlap of the fluorescence spectra of BSA (F) and the absorbance spectra of $(\beta\text{-CD})_2/C_{60}$ (A), c(BSA) = $c[(\beta\text{-CD})_2/C_{60}]$ = 2 μM (298 K).

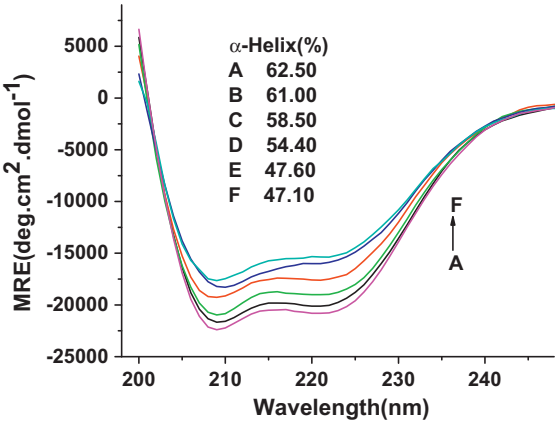

Fig. 11. The CD spectra of $[(\beta\text{-CD})_2/C_{60}]$–BSA system obtained at room temperature and pH 7.4; c(BSA) = 2.0×10^{-6} mol L^{-1}; $c[(\beta\text{-CD})_2/C_{60}]/(2.0 \times 10^{-6}$ mol L$^{-1})$. A–F: 0, 1, 10, 25, 40, 50 respectively.

Energy Transfer) [31] is vividly called "the spectral scale" and is widely used in biological systems. As the intrinsic fluorescence of protein is generated by the tryptophan residues, the efficiency of the energy transfer in biochemistry can be used to evaluate the distance r between the ligand and the tryptophan residues in the protein. According to Förster and Sinanoglu's [32] energy transfer theory, the efficiency of energy transfer between the donor and acceptor, E, could be calculated using equation (Eq. (7)):

$$E = 1 - \frac{F}{F_0} = \frac{R_0^6}{R_0^6 + r^6} \tag{7}$$

where F and F_0 are the fluorescence intensities of BSA in the presence and absence of $(\beta\text{-CD})_2/C_{60}$, r is the distance between donor and acceptor, and R_0 is the critical distance, at which the efficiency of transfer is 50%. R_0 can be calculated by using the following equation (Eq. (8)):

$$R_0^6 = 8.79 \times 10^{-25} K^2 n^{-4} \phi J \tag{8}$$

where K^2 is the orientation factor involved the geometry of the donor–acceptor dipole, n is the refractive index of medium, Φ stands for the donor's fluorescence quantum yield, and J expresses the degree of spectra overlap between the donor's emission and the acceptor's absorption. J is usually calculated by the following equation (Eq. (9)):

$$J = \frac{\int_0^\infty F(\lambda)\varepsilon(\lambda)\lambda^4 \, d\lambda}{\int_0^\infty F(\lambda)\, d\lambda} \tag{9}$$

where $F(\lambda)$ is the fluorescence intensity of the donor at wavelength range λ, $\varepsilon(\lambda)$ is the molar absorption coefficient of the acceptor at the certain wavelength λ. It has been reported that in the biochemistry system, $K^2 = 2/3$, $n = 1.36$, $\Phi = 0.15$, J can be evaluated by integrating the overlap spectra in Fig. 11 according to Eq. (7) while $J = 6.366 \times 10^{-15}$ cm^3 L mol^{-1}. Based on these data, we found $R_0 = 4.08$ nm and $r = 1.1R_0$. Thus, the distance between $(\beta\text{-CD})_2/C_{60}$ and try residue in BSA is about 4.49 nm The donor–acceptor distance ($0.5R_0 < R_0 < 1.5R_0$) [33] and r is in the range of 2–8 nm [34], indicating that the energy transfer from BSA to $(\beta\text{-CD})_2/C_{60}$ occurs with high probability.

3.6. Conformation investigation

3.6.1. Circular dichroism spectroscopy

In order to evaluate the second-structural change in BSA by the addition of $(\beta\text{-CD})_2/C_{60}$, we measured the CD spectra, which are widely used for the determination of the conformational change

Table 4
Fractions of different secondary structures determined by SELCON3.[a]

Molar ratio [(β-CD)$_2$/C$_{60}$)]:[BSA]	$H(r)$ (%)	$H(d)$ (%)	$S(r)$ (%)	$S(d)$ (%)	Trn	Unrd
0:1	42.4	20.1	2.5	2.8	13.0	20.4
1:1	41.0	20.0	2.7	2.8	13.1	20.6
10:1	38.7	19.8	3.2	3.4	14.2	21.0
25:1	34.6	19.8	4.0	4.2	17.2	23.4
40:1	29.1	18.5	4.9	5.4	18.8	25.6
50:1	28.9	18.2	6.1	5.5	18.5	23.8

$H(r)$, regular α-helix; $H(d)$, distorted α-helix; $S(r)$, regular β-strand; $S(d)$, distorted β-strand; Trn, turns; Unrd, unordered structure.

in proteins and polypeptides in solution. The CD spectra of BSA with various concentration of (β-CD)$_2$/C$_{60}$ in PBS and at room temperatures are shown in Fig. 11, the contents of different types of secondary structures were analyzed by the algorithm SELCON3. The scan speed was set as speed of 200 nm/min and the signal was the average of three scans. The concentration of BSA was fixed at 2 mM. Far-UV CD spectra of BSA were recorded from 200 to 250 nm. The contents of free and combined BSA were calculated from the MRE value at 208 nm using the following equation [35] (Eq. (10)):

$$\alpha\text{-Helix}\ \ (\%) = \frac{-\mathrm{MRE}_{208} - 400}{33,000 - 4000} \qquad (10)$$

where MRE_{208} is the MRE value observed at 208 nm, 4000 is the MRE of β-form and random coil conformation cross at 208 nm and 33,000 is the MRE value of a pure α-helix at 208 nm. The contents of α-helix and β-strand are calculated by using SELCON3. The results are listed in Table 4.

It is seen that BSA exhibits two negative bands at 208 nm and 222 nm, which represent the typical α-helix structure of protein. After the titration of (β-CD)$_2$/C$_{60}$, the helicity of BSA decreased significantly and the β-strands, turn, and unordered structure increased slightly. As known, the secondary structure contents are related closely to the biological activity of protein, thus a decrease in α-helix from 62.5 to 47.1% means the loss of the biological activity of

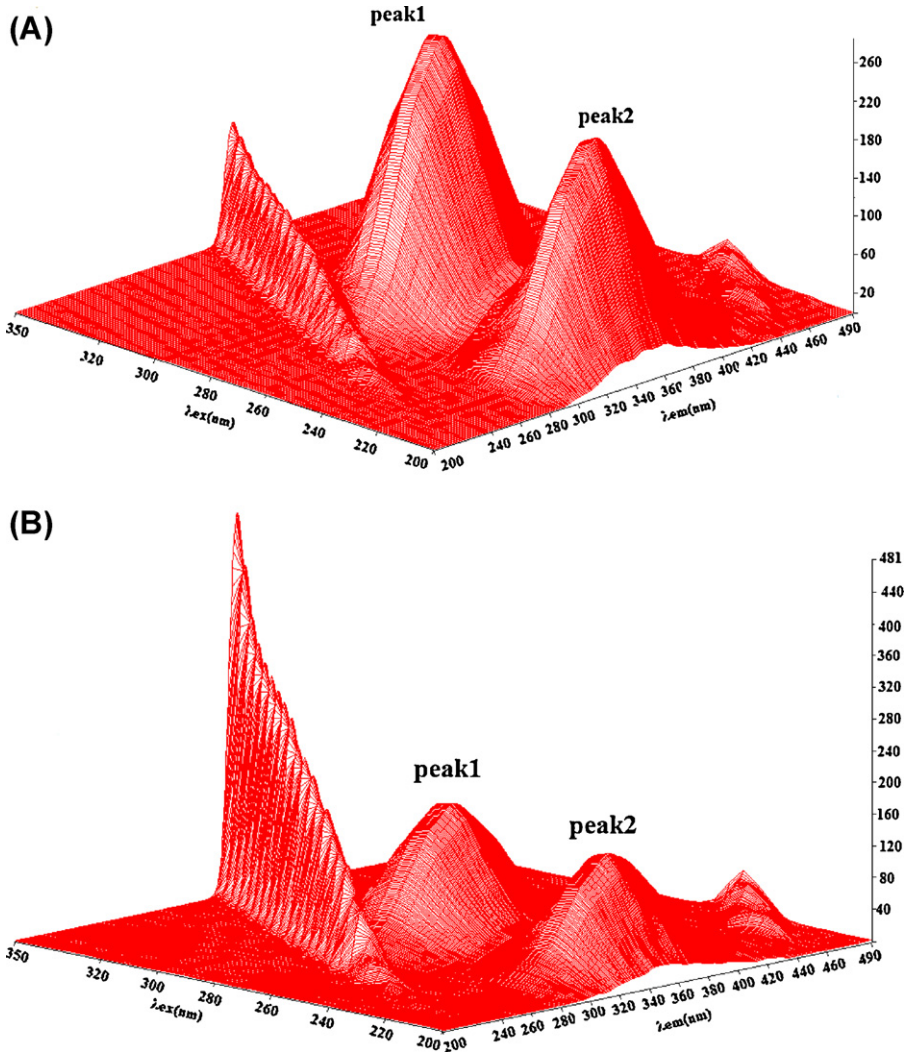

Fig. 12. Three-dimensional fluorescence spectra of BSA (A) and [(β-CD)$_2$/C$_{60}$]–BSA complex (B), c(BSA) = c[(β-CD)$_2$/C$_{60}$] = 2 μM (298 K).

BSA upon interaction with a higher concentration of $(\beta\text{-CD})_2/C_{60}$, which also suggests a structural change that is related to a low degree of surface coverage [36].

3.6.2. Three-dimensional fluorescence spectroscopy

For further insight into the conformation change in BSA by the addition of the water-soluble nanomaterial of fullerene, the three-dimensional fluorescence spectra offers another valuable method to monitor the changes in the secondary structure of protein and their dynamics. Fig. 12(A) and (B) shows the three-dimensional fluorescence spectra of BSA and $[(\beta\text{-CD})_2/C_{60}]$–BSA, with the λ_{ex} = 200–330 nm and λ_{em} = 200–500 nm respectively. Two peak regions (peak 1 at 285 nm/350 nm and peak 2 at 225 nm/348 nm) were observed. Peak 1 shows the spectral characteristics of tryptophan and tyrosine residues, and peak 2 is related to changes the conformation of the peptide backbone [37]. Fig. 12 shows that both of fluorescence peaks in the three-dimensional fluorescence spectra of BSA are quenched, and peak 2 is changes greater than peak 1, altering the peptide backbone, tryptophan and tyrosine residues and the conformations (see also Fig. S7). Combining the three-dimensional fluorescence quenching and the CD spectra results, we can conclude that a specific interaction occurs between BSA and $[(\beta\text{-CD})_2/C_{60}]$ and $(\beta\text{-CD})_2/C_{60}$ can be combined with BSA to change its conformation.

4. Conclusion

In this paper, one water-soluble derivative of fullerene was synthesized by an improved method through encapsulating, which was determined by elemental analysis, SEM, IR, TG-DSC, UV–vis, XRD and ^{13}C NMR. The interaction between $(\beta\text{-CD})_2/C_{60}$ and BSA was characterized by spectroscopy and electrochemical methods. The study demonstrates that the interaction between $(\beta\text{-CD})_2/C_{60}$ and BSA is mainly the static quenching mechanism. Site marker competitive experiments indicate that the binding of $(\beta\text{-CD})_2/C_{60}$ to BSA primarily took place in sub-domain IIA. Electrostatic interactions played an important role in the quenching process, and the binding process of $(\beta\text{-CD})_2/C_{60}$ could induce the conformation change in BSA. In addition, a π–π stacking interaction could also play an important role in binding, as π–π stacking may be a general mode for the interaction of fullerenes and their derivatives with proteins [38]. Furthermore, the current study should help the understanding of how water soluble nanomaterials interact with native proteins at the molecular level under near physiological conditions and shed light on the mystery of investigation the application potentials of nanomaterials, such as fullerene derivatives, in biology.

Acknowledgements

We gratefully acknowledge financial support from the Program for Changjiang Scholars and Innovative Research Team in University (IRT1030), the National Natural Science Foundation of China (21077081, 20921062), the Natural Science Foundation of Hubei Province (2010CDB01302) and the Fundamental Research Funds for Central Universities (1103005).

Appendix A. Supplementary data

Supplementary data associated with this article can be found, in the online version, at doi:10.1016/j.jphotochem.2011.11.009.

References

[1] D. Francois, G.L. Marcos, Supramolecular fullerene chemistry, Chem. Soc. Rev. 28 (1999) 263–277.
[2] C.Y. Usenko, S.L. Harper, R.L. Tanguay, Exposure to C_{60} elicits an oxidative stress response in embryonic zebrafish, Toxicol. Appl. Pharmacol. 229 (2008) 44–55.
[3] R. Sijbesma, G. Srdanov, F. Wudl, J.A. Castoro, C. Wilkins, S.H. Friedman, D.L. DeCamp, G.L. Kenjon, J. Am. Chem. Soc. 115 (1993) 6506–6510.
[4] X.F. Zhang, C.Y. Shu, L. Xie, C.R. Wang, Y.Z. Zhang, J.F. Xiang, L. Li, Y.L. Tang, Protein conformation changes induced by a novel organophosphate-containing water-soluble derivative of a C_{60} fullerene nanoparticle, J. Phys. Chem. C 111 (2007) 14327–14333.
[5] S.H. Friedman, D.L. DeCamp, R.P. Sijbesma, G. Srdanov, F. Wudl, G.L. Kenyon, Inhibitions of the HIV-1 protease by fullerene derivatives: model building studies and experimental verification, J. Am. Chem. Soc. 115 (1993) 6506–6509.
[6] E. Nakamura, H. Isobe, Functionalized fullerenes in water. The first 10 years of their chemistry, biology, and nanoscience, Acc. Chem. Res. 36 (2003) 807–815.
[7] L.Y. Chiang, J.B. Bhonsle, L. Wang, S.F. Shu, T.M. Chang, J.R. Hwu, Efficient one-flask synthesis of water-soluble C_{60} fullerenols, Tetrahedron 52 (1996) 4963–4972.
[8] A. Kumar, M.V. Rao, S.K. Menon, Photoinduced DNA cleavage by fullerene–lysine conjugate, Tetrahedron Lett. 50 (2009) 6526–6530.
[9] M.V. Rekharsky, Y. Inoue, ChemInform abstract: complexation thermodynamics of cyclodextrins, Chem. Rev. 98 (1998) 1875–1917.
[10] L. Shang, X. Jiang, S. Dong, In vitro study on the binding of neutral red to bovine serum albumin by molecular spectroscopy, J. Photochem. Photobiol. A 184 (2006) 93–97.
[11] Z.D. Qi, B. Zhou, Q. Xiao, C. Shi, Y. Liu, J. Dai, Interaction of rofecoxib with human serum albumin: Determination of binding constants and the binding site by spectroscopic methods, J. Photochem. Photobiol. A 193 (2008) 81–88.
[12] X.M. He, D.C. Carter, Atomic structure and chemistry of human serum albumin, Nature 358 (1992) 209–215.
[13] Y.Y. Gao, L.H. Liu, Z.Z Ou, Y. Li, G.Q. Yng, X.S. Wang, Biological activity of a cholesterol modified fullerene/γ-cyclodextrin inclusion complex, Acta. Phys.: Chim. Sin. 26 (2010) 495–501.
[14] G.C. Zhao, P. Zhang, X.W. Wei, Z.S. Yang, Determination of proteins with fullerol by a resonance light scattering technique, Anal. Biochem. 334 (2004) 297–302.
[15] B. Belgorodsky, L. Fadeev, J. Kolsenik, M. Gozin, Formation of a soluble stable complex between pristine C_{60}–fullerene and a native blood protein, Chem. Biol. Chem. 7 (2006) 1783–1789.
[16] W. Liu, Y. Zhang, X. Gao, Interfacial supramolecular self-assembled monolayers of C_{60} by thiolated α-cyclodextrin on gold surfaces via monoanionic C_{60}, J. Am. Chem. Soc. 129 (2007) 4973–4980.
[17] Y. Zhang, W. Liu, X. Gao, Y. Zhao, M. Zheng, F. Li, D. Ye, The first synthesis of a water-soluble [alpha]-cyclodextrin/C_{60} supramolecular complex using anionic C_{60} as a building block, Tetrahedron Lett. 47 (2006) 8571–8574.
[18] F. Adrian, T. Budtova, E. Tarabukina, M. Pinteala, S. Mariana, C. Peptu, V. Harabagiu, B.C. Simionescu, Inclusion complexes of α-cyclodextrin and carboxyl-modified α-cyclodextrin with C_{60}: synthesis, characterization and controlled release application via microgels, J. Incl. Phenom. Macrocycl. Chem. 64 (2009) 83–94.
[19] P. Boulas, W. Kutner, M.T. Jones, K.M. Kadish, Bucky (basket) ball: stabilization of electrogenerated C_{60}. bul.-radical monoanion in water by means of cyclodextrin inclusion chemistry, J. Phys. Chem. 98 (1994) 1282–1287.
[20] F.L. Cui, J.L. Wang, Y.R. Cui, J.P. Li, Fluorescenct investigation of the interactions between N-(p-chlorophenyl)-N′-(1-naphthyl) thiourea and serum albumin: synchronous fluorescence determination of serum albumin, Anal. Chim. Acta 571 (2006) 175–183.
[21] Y.J. Hu, Y. Ou-Yang, C.M. Dai, Y. Liu, X.H. Xiao, Site-selective binding of human serum albumin by palmatine: spectroscopic approach, Biomacromolecules 11 (2009) 106–112.
[22] J.R. Lakowicz, Principles to Fluorescence Spectroscopy, Plenum, New York, 2006, pp. 278, 281, 283, 13.
[23] B.K. Sahoo, K.S. Ghosh, S. Dasgupta, Molecular interactions of isoxazolcurcumin with human serum albumin: spectroscopic and molecular modeling studies, Biopolymers 91 (2009) 108–119.
[24] K. Tawa, D. Yao, W. Knoll, Matching base-pair number dependence of the kinetics of DNA–DNA hybridization studied by surface plasmon fluorescence spectroscopy, Biosens. Bioelectron. 21 (2005) 322–329.
[25] Q.L. Zhang, Y.N. Ni, S. Kokot, Molecular spectroscopic studies on the interaction between Ractopamine and bovine serum albumin, J. Pharm. Biomed. Anal. 52 (2010) 280–288.
[26] D. Leckband, Measuring the forces that control protein interactions, Annu. Rev. Biophys. Biomol. Struct. 29 (2000) 1–26.
[27] J.B. Xiao, J.W. Chen, H. Cao, F.L. Ren, C.S. Yang, Y. Chen, M. Xu, Study of the interaaction between baicalin and bovine serum albumin by multi-spectroscopic method, J. Photochem. Photobiol. A 191 (2007) 222–227.
[28] B. Sandhya, A.H. Hegde, S.S. Kalanur, U. Katrahalli, J. Seetharamappa, Interaction of triprolidine hydrochloride with serum albumins: Thermodynamic and binding characteristics, and influence of site probes, J. Pharm. Biomed. Anal. 54 (2011) 1180–1186.
[29] G. Sudlow, D. Birkett, D. Wade, The characterization of two specific drug binding sites on human serum albumin, Mol. Pharmacol. 11 (1975) 824.
[30] Y.V. Il'ichev, J.L. Perry, J.D. Simon, Interaction of ochratoxin A with human serum albumin: preferential binding of the dianion and pH effects, J. Phys. Chem. B 106 (2002) 452–459.
[31] L. Stryer, Fluorescence energy transfer as a spectroscopic ruler, Annu. Rev. Biochem. 47 (1978) 819–846.

[32] T. Förster, Intermolecular energy migration and fluorescence, Ann. Phys. 2 (1948) 55–75.
[33] B. Valeur, Molecular Fluorescence: Principles and Applications, Wiley Press, New York, 2001.
[34] S. Weiss, Fluorescence spectroscopy of single biomolecules, Science 283 (1999) 1676.
[35] P.B. Kandagal, J. Seetharamappa, S.M.T. Shaikh, D.H. Manjunatha, Binding of trazodone hydrochloride with human serum albumin: a spectroscopic study, J. Photochem. Photobiol. A 185 (2007) 239–244.
[36] Q. Xiao, S. Huang, Z.D. Qi, B. Zhou, Z.K. He, Y. Liu, Conformation, thermodynamics and stoichiometry of HSA adsorbed to colloidal CdSe/ZnS quantum dots, Biochim. Biophys. Acta 1784 (2008) 1020–1027.
[37] Y.Z. Zhang, B. Zhou, Y.X. Liu, C.X. Zhou, X.L. Ding, Y. Liu, Fluorescence study on the interaction of bovine serum albumin with p-aminoazobenzene, J. Flouresc. 18 (2008) 109–118.
[38] S.T. Yang, H. Wang, L. Guo, Y. Gao, Y. Liu, A. Cao, Interaction of fullerenol with lysozyme investigated by experimental and computational approaches, Nanotechnology 19 (2008) 395101.